ICOLD Symposium on Sustainable Development of Dams and River Basins, 24th - 27th February, 2021, New Delhi

A 1D-2D COUPLED LATTICE BOLTZMANN MODEL FOR SHALLOW WATER SIMULATIONS IN LARGE SCALE RIVER-LAKE SYSTEMS

J. Y. WUA
Changjiang Institute of Survey, Planning, Design and Research, Wuhan, China
State Key Laboratory of Water Resources and Hydropower Engineering Science, Wuhan University, Wuhan, China

A. Q. LIA AND L. M. ZHANGA
Changjiang Institute of Survey, Planning, Design and Research, Wuhan, China

ABSTRACT

Simulating shallow water flows in large scale river-lake systems is important but challenging because huge computer resources and time are needed. Among many numerical schemes, the newly developed lattice Boltzmann (LB) method is attractive, because of its easy implementation, intrinsic parallelism, and high accuracy. This paper aims to propose a simple and efficient 1D-2D coupled LB model for simulating these flows, with the main focus on the coupling strategy of the 1D-2D interfaces. The coupling strategy is implemented at the mesoscopic level, in which the unknown distribution functions in the LB equation are calculated from the known distribution functions and the primitive variables at the adjacent lattice nodes. To verify the numerical accuracy and stability, two typical cases, namely, the dam break flow and the surge waves in the tailrace canal of a hydropower station, are simulated by the 1D-2D coupled LB model. The results agree well with both analytical solutions and commercial software results. To further demonstrate its capability, the model is used to simulate the surge wave propagation and reflection phenomena in the reservoir of a run-of-river hydropower station. The flow characteristics are illustrated, and the high efficiency is proved. It is evident that the 1D-2D coupled LB model is accurate and reliable in simulating practical large-scale river-lake systems.

***Keywords**: shallow water flows; 1D-2D coupled model; lattice Boltzmann method; large-scale simulation; river-lake systems.*

INTRODUCTION

One-dimensional (1D) and two-dimensional (2D) shallow water equations are widely used to simulate flows in rivers, lakes, reservoirs, and estuaries. The dimensionally different models are suitable for different scenarios. The cross-sectional integrated 1D models are extremely suitable for hydrodynamic simulations in large scale river networks, with their lumped boundary representations for hydraulic structures such as weirs, dams, culverts, and pumps. On the other hand, 2D models, with their ability to accurately resolve flows in both longitudinal and transversal directions, are the primary choice for hydrodynamic simulations for lakes, reservoirs, and estuaries. Because 1D river networks and 2D lakes are often linked together, it is natural to choose the 1D-2D coupled model for accurately investigating their interactions.

Currently, the numerical solvers for the shallow water equations are mainly based on traditional methods, such as implicit finite-difference scheme for the 1D model, and finite-volume method for the 2D model [1–3]. Even if being accepted widely, these traditional methods are relatively difficult to implement, and the calculations are usually time-consuming. Recently, the lattice Boltzmann (LB) method is developed for simulating complicated fluid flow problems, such as multi-dimensional hydrodynamic flows, multiphase flows, and multi-component flows. Its easy implementation, intrinsic parallelism, and high accuracy have been demonstrated by many works [4–7]. Because of these advantages, introducing LB method into simulations of the shallow water flows seems to be very attractive. Cheng [8,9] first introduced the 1D LB model for the 1D shallow water equations, and Frandsen [10] had further verified the model. Later, Thang [11] used it to simulate flows in complex irrigation channels, and Chopard [12] used it to simulate flows in rapids canals. On the other hand, Zhou [13] first developed a 2D LB model for the shallow water equations, in which the terrain and riverbed friction are represented by source terms in the original LB equation. Cheng and Zhang [14,15] used a similar 2D LB model to simulate the surge propagations caused by the transient processes of hydropower stations. Liu [16–19] adopted the 2D models to simulate flows in open channels and shallow lakes.

This paper aims to propose a 1D-2D coupled LB model for simulating shallow flows in river-lake systems. Thus, it is necessary to discuss the 1D-2D coupling strategies. According to the specific problems, the strategies are mainly divided into three categories: the lateral coupling, the superposition coupling, and the boundary connected coupling [20]. The first category is mainly adopted to simulate flows in floodplain systems [2,21]. The second category is mainly used to simulate flows in systems with obvious 2D flow effects of local flow patterns, in which the high-dimensional model is superimposed on the low-dimensional global model [22,23]. The third category is mainly applied to rivers, lakes, reservoirs, and estuarine systems, which connect different dimensional models directly through the coupling boundaries. There are a variety of coupling strategies available for the third category. The simplest one is to run each submodel in sequence, with its boundary conditions provided by the previous solution of each other [24–26]. However, the mutually provided boundary conditions are lagged, causing the non-conservation of mass or momentum. To reduce the errors, overlapped areas are set at the coupling boundaries [27–29], but it still cannot avoid the errors caused by the lagged boundary conditions. Another strategy is to use iterative methods to solve the coupling boundaries, which can fully meet the conservation of mass and momentum [20]. However, each iteration must go through an overall calculation, and one time step may need several iterations, resulting in a great calculation amount and a low computational efficiency.

The coupling strategies listed above are tailored for traditional numerical methods. However, the works addressing the coupling procedure of interconnected subdomains for the LB based shallow water simulations are rare. We found only one similar work tried to couple 2D LB shallow water model with 2D LB free-surface model [29], but the coupling strategy was still implemented at the macroscopic level, and the numerical stability was affected by both relaxation time and the size of the overlapping region.

Here, we present a rather simple and efficient 1D-2D coupled LB model, with a coupling strategy at the mesoscopic level. The coupling interface is regarded as an interior node with only three unknown distribution functions to be solved, and the numerical stability is only affected by the relaxation time. Moreover, the proposed model retains all the merits of the LB method [30,31], especially its intrinsic parallelism and easy programming, making it quite suitable for hydrodynamic simulations in large scale river-lake systems.

The paper is organized as follows. The 1D-2D coupled LB model is described in Section 2. Two typical cases are simulated to verify the proposed model in Section 3. An application to simulating the surge wave propagation and reflection processes in a practical run-of-river hydropower station is presented in Section 4. Finally, a brief conclusion is made to end the article.

1D and 2D lattice Boltzmann models and their coupling strategy

1D LB model

The common LB equation [9] with Bhatnagar-Gross-Krook (BGK) collision operator can be written as

$$f_\alpha(\boldsymbol{x}+\boldsymbol{e}_\alpha\Delta t, t+\Delta t)-f_\alpha(\boldsymbol{x},t)=-\frac{1}{\tau}\left[f_\alpha(\boldsymbol{x},t)-f_\alpha^{eq}(\boldsymbol{x},t)\right]+F_\alpha,(\alpha=0,1,2) \tag{1}$$

where the left side terms of Eq. (1) denote the propagation process, and the right side terms of Eq.(1) denote the collision process; $\boldsymbol{x}$ is the lattice node coordinate; $\boldsymbol{e}_\alpha$ is the discrete particle velocity; $f_\alpha(\boldsymbol{x},t)$ is the discrete distribution function along the αth particle velocity direction, and $f_\alpha^{eq}(\boldsymbol{x},t)$ is its corresponding equilibrium; τ is the relaxation time; F_α is the external forcing term.

Here, the D1Q3 model is adopted, in which the three discrete particle velocities are $\{e_2,e_0,e_1\}=c\cdot\{-1,0,1\}$, with the lattice speed $c=\Delta x/\Delta t$. The equilibrium distribution functions can be expressed as

$$f_0^{eq}=h-\frac{gh^2}{2c^2}-\frac{hu^2}{c^2},\ f_1^{eq}=\frac{gh^2}{4c^2}+\frac{hu}{2c}+\frac{hu^2}{2c^2},\ f_2^{eq}=\frac{gh^2}{4c^2}-\frac{hu}{2c}+\frac{hu^2}{2c^2} \tag{2}$$

Water depth and velocity of the fluid are calculated by the moments of mesoscopic variable $f_\alpha(\boldsymbol{x},t)$

$$h=\sum_\alpha f_\alpha,\ h\boldsymbol{u}=\sum_\alpha \boldsymbol{e}_\alpha f_\alpha \tag{3}$$

The second-order treatment of external forcing term proposed by Cheng [9] is adopted, and F_α can be written as

$$F_1=\frac{gh}{2}\left(\frac{\partial z}{\partial x}-S_f\right),\ F_0=0,\ F_2=-\frac{gh}{2}\left(\frac{\partial z}{\partial x}-S_f\right) \tag{4}$$

where h is the water depth, u is the velocity, g is the gravitational acceleration, z is the water surface elevation, S_f is the frictional loss.

The simulation results of the LB model should be approximate to the solution to the 1D Saint Venant equations. The LB model can recover the corresponding macroscopic 1D shallow water Eqs. (5) and (6) by the Chapman-Enskog expansion [9].

$$\frac{\partial h}{\partial t}+\frac{\partial(hu)}{\partial x}=0 \tag{5}$$

$$\frac{\partial(hu)}{\partial t}+\frac{\partial}{\partial x}\left(hu^2+\frac{gh^2}{2}\right)=gh\left(\frac{\partial z}{\partial x}-S_f\right) \tag{6}$$

As for boundary treatment, the unknown distribution functions at inlet and outlet boundary can be defined as

Inlet boundary: $f_1=h-f_0-f_2$, or $f_1=\dfrac{(1+u)f_2+uf_0}{1-u}$ (7)

Outlet boundary: $f_2=h-f_0-f_1$, or $f_2=\dfrac{(1-u)f_1+uf_0}{1+u}$ (8)

2D LB model

The 2D LB equation [32] can be written as

$$f_\alpha(\boldsymbol{x}+\boldsymbol{e}_\alpha\Delta t,t+\Delta t)-f_\alpha(\boldsymbol{x},t)=\Omega_\alpha+F_\alpha \tag{9}$$

where Ω_α is the collision operator, the definition of other variables are the same as Eq. (1).

The D2Q9 model are applied, and the discrete particle velocities are

$$\boldsymbol{e}_\alpha = c \cdot \begin{Bmatrix} 0 & 1 & -1 & 0 & 0 & 1 & -1 & 1 & -1 \\ 0 & 0 & 0 & 1 & -1 & 1 & -1 & -1 & 1 \end{Bmatrix} \tag{10}$$

The equilibrium distribution functions are expressed as

$$\begin{cases} f_\alpha^{eq} = h - \dfrac{5gh^2}{6c^2} - \dfrac{2h}{3c^2}\boldsymbol{u}^2, \ \alpha = 0 \\ f_\alpha^{eq} = w_\alpha \cdot \dfrac{h}{c^2} \cdot \left(\dfrac{3}{2}gh + 3\boldsymbol{e}_\alpha \cdot \boldsymbol{u} + \dfrac{9}{2c^2}(\boldsymbol{e}_\alpha \cdot \boldsymbol{u})^2 - \dfrac{3}{2}\boldsymbol{u}^2\right), \alpha = 1,2,\ldots,8 \end{cases} \tag{11}$$

where the weight factor $w_\alpha = \{4/9, 1/9, 1/9, 1/9, 1/9, 1/36, 1/36, 1/36, 1/36\}$.

The multi-relaxation time (MRT) collision operator is adopted [32]. Compared with the single-relaxation-time (SRT) LB, the MRT-LB incorporates more fluid physical information and is more stable and accurate. Water depth and velocity of the fluid can be calculated by Eq. (3).

In this study, we follow Cheng [33] in treating the external forcing term F_α. Assuming the A is the source term in the continuity Eq. (14) and $\boldsymbol{B}$ is the external forcing term in the momentum Eq. (15), the F_α can be written as

$$F_\alpha = \frac{1}{2}\Delta t\left[q_\alpha(\boldsymbol{x} + \boldsymbol{e}_\alpha \Delta t, t + \Delta t) + q_\alpha(\boldsymbol{x}, t)\right] \tag{12}$$

$$q_\alpha = w_\alpha \left\{A + 3\boldsymbol{B} \cdot \left[(\boldsymbol{e}_\alpha - \boldsymbol{u}) + 3(\boldsymbol{e}_\alpha \cdot \boldsymbol{u})\boldsymbol{e}_\alpha\right]\right\} \tag{13}$$

in which $A = 0$, $\boldsymbol{B} = \boldsymbol{S}$.

With the above setups, this 2D LB model can recover 2D shallow water Eqs. (14) and (15) by the Chapman-Enskog expansion in the incompressible flow limit [34].

$$\frac{\partial h}{\partial t} + \frac{\partial (hu_j)}{\partial x_j} = 0 \tag{14}$$

$$\frac{\partial (hu_i)}{\partial t} + \frac{\partial (hu_i u_j)}{\partial x_j} = -\frac{\partial}{\partial x_i}\left(\frac{g}{2}h^2\right) + \nu \frac{\partial^2 (hu_j)}{\partial x_j \partial x_j} + \boldsymbol{S} \tag{15}$$

where u_i and u_j is the depth-averaged velocities; $\boldsymbol{S} = \boldsymbol{S}_b - \boldsymbol{S}_f$, with $\boldsymbol{S}_b = \boldsymbol{g}hP_b$ is the hydraulic gradient caused by the bed gradient, with P_b is the component of bed gradient; $\boldsymbol{S}_f = \boldsymbol{g}un^2\sqrt{u_j u_j} / \sqrt[3]{h}$ is the hydraulic gradient caused by bed shear stresses, with n is the coefficient of Manning.

The Coupling strategy of 1D-2D coupled LB model

The coupling interface is in the form of a node in the 1D computational domain, and in the form of a line in the 2D computational domain. In the present study, it is treated as an interior node at the 1D domain, with three unknown distribution functions to be calculated. These unknown distribution functions at the coupling interface are calculated by the distribution functions from the adjacent 1D and 2D nodes. The reformulation of the unknown distribution function is depicted in **Fig. 1**, in which g_α denote distribution functions of the 1D domain, f_α denote distribution functions of the 2D domain, k refers to the position of the coupling

node at the 1D domain; j refers to time, and m denotes the position of the coupling node at the 2D domain.

The processing steps for dealing coupling interface can be expressed as follows:

(1) Calculate the three unknown distribution functions at the coupling interface;

(2) Calculate the water depth and velocity of the coupling interface by the distribution functions that solved in the first step;

(3) Calculate the unknown distribution functions of the 2D domain at the interface by macroscopic parameters.

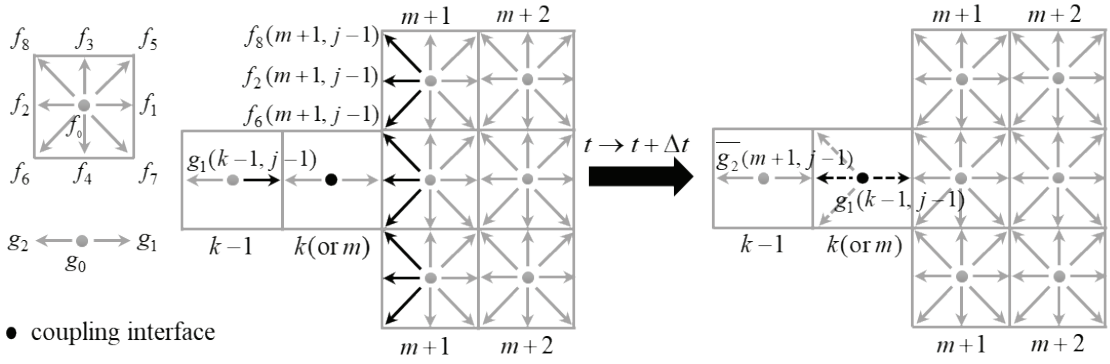

Fig. 1. Sketch of the 1D-2D LB coupling boundary.

To be specific, as shown in **Fig. 1**, the unknown distribution functions $g_0(k,j)$, $g_1(k,j)$, $g_2(k,j)$ at the coupling boundary are calculated at first.

$g_1(k,j)$ can be expressed as

$$g_1(k,j) = g_1(k-1,j-1) - \frac{1}{\tau}(g_1(k-1,j-1) - g_1^{eq}(k-1,j-1)) + F_1 \tag{16}$$

$g_2(k,j)$ can be calculated by the distribution functions at the adjacent 2D nodes and expressed as

$$g_2(k,j) = \overline{g_2}(m+1,j-1) - \frac{1}{\tau}(\overline{g_2}(m+1,j-1) - g_2^{eq}(m+1,j-1)) + F_2 \tag{17}$$

Where $\overline{g_2}(m+1,j-1) = \overline{f_2}(m+1,j-1) + \overline{f_6}(m+1,j-1) + \overline{f_8}(m+1,j-1)$, with $\overline{f_2}(m+1,j-1)$, $\overline{f_6}(m+1,j-1)$, and $\overline{f_8}(m+1,j-1)$ are the averaged values of distribution functions at position m+1.

$g_0(k,j)$ can be calculated by

$$g_0(k,j) = g_0(k,j-1) - \frac{1}{\tau}(g_0(k,j-1) - g_0^{eq}(k,j-1)) + F_0 \tag{18}$$

Then, the water depth and velocity can be obtained by

$$h(k,j) = g_1(k,j) + g_2(k,j) + g_0(k,j) \tag{19}$$

$$u(k,j) = (g_1(k,j) - g_2(k,j))/h(k,j) \tag{20}$$

Finally, given $h_{in} = h(k, j)$, $u_x = u(k, j)$, $u_y = 0$, assuming that $f_1 - f_1^{eq} = f_2 - f_2^{eq}$. The unknown distribution functions f_1, f_5, and f_7 at the inlet boundary of the 2D domain is solved by Eq. (21).

$$\begin{cases} f_1 = f_2 + \dfrac{2}{3} h_{in} u_x / c \\ f_5 = f_6 - \dfrac{1}{2}(f_3 - f_4) + \dfrac{1}{2} h_{in} u_y / c + \dfrac{1}{6} h_{in} u_x / c \\ f_7 = f_8 + \dfrac{1}{2}(f_3 - f_4) - \dfrac{1}{2} h_{in} u_y / c + \dfrac{1}{6} h_{in} u_x / c \end{cases} \tag{21}$$

Similarly, the unknown distribution functions f_2, f_6, and f_8 at the outlet boundary of the 2D domain can be solved by Eq. (22). Other boundaries of the 2D domain are regarded as no-slip solid walls and treated by non-equilibrium rebound scheme [35].

$$\begin{cases} f_2 = f_1 - \dfrac{2}{3} h_{out} u_x / c \\ f_6 = f_5 + \dfrac{1}{2}(f_3 - f_4) - \dfrac{1}{2} h_{out} u_y / c - \dfrac{1}{6} h_{out} u_x / c \\ f_8 = f_7 - \dfrac{1}{2}(f_3 - f_4) + \dfrac{1}{2} h_{out} u_y / c - \dfrac{1}{6} h_{out} u_x / c \end{cases} \tag{22}$$

The above coupling strategy is aimed at conditions that the 1D model is adopted at upstream and the 2D model is adopted at downstream. The processing steps for conditions that the 2D model is adopted at upstream and the 1D model is adopted at downstream are solved in the same way. In this case, the coupling interface is at the outlet boundary, which is regarded as an interior node at the 1D domain. The three steps mentioned above is used to solve the unknown distribution functions of the coupling interface. Eqs. (21) and (22) are used to calculate the unknown distribution functions at the inlet boundary and the outlet boundary for the 2D domain, respectively.

Accuracy and stability verification

To verify the accuracy and stability of the 1D-2D coupled LB model, the dam break flow and the surge wave flow in the tailrace canal of a hydropower station are simulated.

The dam break flow

The dam break flow in a frictionless and flat rectangular channel is simulated. As shown in **Fig. 2**, the dam is placed across the channel at the middle plane of the domain, and the initial water depths at the upstream and downstream sides are set to 8 m and 2 m, respectively. The initial velocity is zero. When the dam collapses completely in a sudden, two bores propagating in the upstream and downstream directions, respectively, are generated. In the simulation setup, the channel is divided into three domains, with the middle domain simulated by the 2D LB model, and the two outer domains simulated by the 1D LB model (**Fig. 2**). The upstream and downstream boundaries are set as constant water depths. x_1 and x_2 denote the coupling interfaces, and the side boundaries of the 2D domain are treated as no-slip walls. Like any other explicit numerical methods, the 1D-2D coupled LB model must satisfy the stability requirements:

$$Cn = \frac{|u|}{|c|} \le 1.0, \quad Fr = \frac{|u|}{\sqrt{gh}} \le 1.0, \quad \frac{Cn}{Fr} = \frac{\sqrt{gh}}{|c|} \le 1.0 \tag{23}$$

in which Cn is Courant number, and Fr is Froude number.

The accuracy of the 1D-2D coupled LB model is analyzed by comparing the results of 1D LB, 2D LB, 1D-2D LB, and analytic solution [36]. The lattice length is set to 0.2 m and time step is 0.01 s, and the relaxation time for the 1D model is 0.8, the 2D model is 1.0, and the 1D-2D model, with tau1_up=0.8 is set for the upstream 1D model, tau1_down=0.85 for the downstream 1D model, and tau2=1.4 for the 2D model. Note these relaxation time parameters set for the 1D-2D LB model are optimized and regarded as the default values in the rest of this paper unless otherwise specified.

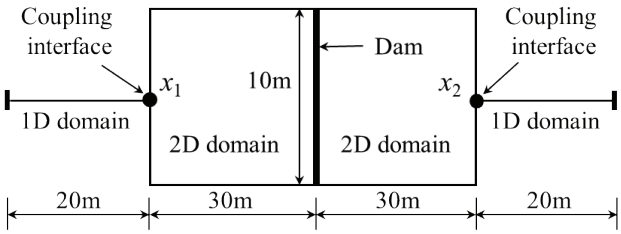

Fig. 2. Computational domain of the dam break case.

Accuracy analysis

Fig. 3 compares the profiles of water depth and velocity of the present method with those obtained by 1D LB, 2D LB, and analytic solutions. The wave front passes through the interface, but the shape doesn't change in all cases. The numerical results of the three numerical models almost coincide with each other and agree well with the analytic solutions. Besides, the errors of the proposed model are slightly larger than those of 1D and 2D models, but still within a very small range. The difference values of maximum relative error between the proposed model and 1D and 2D models are within 3.5%.

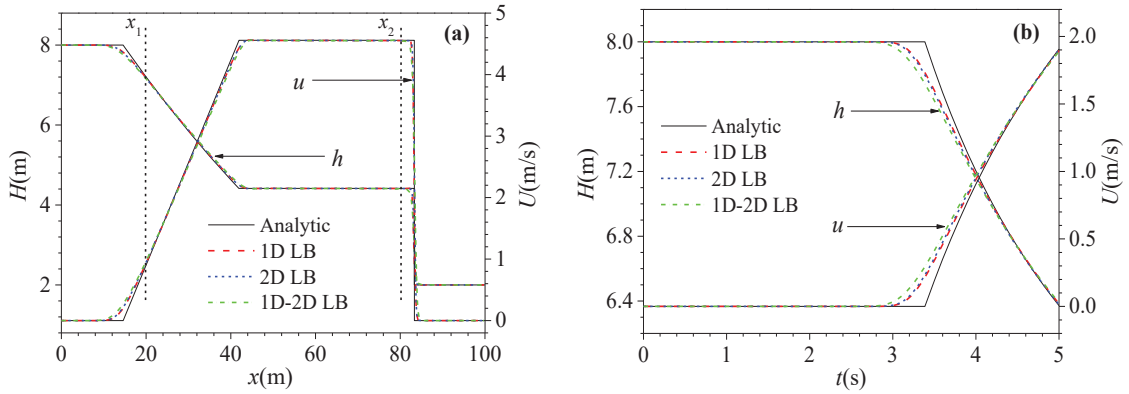

Fig. 3. Simulated results of different models and comparison with the analytic solution: (a) water depth and velocity profiles at t=4.0 s; (b) water depth and velocity histories at coupling interface x_1.

Table 1 : Errors at coupling interfaces x_1 and x_2 of the three models at t=4.0 s (absolute error (AE), relative error (RE)).

Methods	x_1			x_2		
	h (m)	AE (m)	RE (%)	h (m)	AE (m)	RE (%)
Analytic	7.203	-	-	4.414	-	-
1D LB	7.179	0.024	0.34	4.411	0.003	0.06
2D LB	7.168	0.035	0.49	4.411	0.003	0.06
1D-2D LB	7.155	0.048	0.67	4.408	0.006	0.13
Methods	u (m/s)	AE (m/s)	RE (%)	u (m/s)	AE (m/s)	RE (%)
Analytic	0.906	-	-	4.557	-	-
1D LB	0.939	0.034	3.70	4.552	0.005	0.10
2D LB	0.952	0.047	5.14	4.552	0.005	0.10
1D-2D LB	0.970	0.064	7.05	4.549	0.008	0.17

shows the errors of three numerical models at x_1 and x_2, respectively. The errors of the 1D-2D coupled LB model are quite small. The absolute errors for water depth are within 0.05m, and the relative errors are within 1%. The errors for velocity is a little larger, with a maximum absolute error of 0.064 m/s, which is acceptable in practical engineering. Besides, the errors of the proposed model are slightly larger than those of 1D and 2D models, but still within a very small range. The difference values of maximum relative error between the proposed model and 1D and 2D models are within 3.5%.

Convergence analysis

To study grid convergence of the present model, we keep the normalized parameters unchanged and refine the mesh. As shown in **Fig. 4**, the results approach analytic solution as the mesh becomes finer. But as the mesh becomes very fine, such as mesh sizes 0.1 m and 0.2 m, the differences between their results are very small. As shown in **Table 2**, the relative errors of water depth at the coupling interfaces for mesh sizes 0.1 m and 0.2 m are both within 1%, and the relative errors of velocity are within 5%. But the relative errors of mesh size 0.4 m are much larger, with a maximum value of 13%. Therefore, to get an accurate solution at the coupling interfaces (H_{RE}<5% and V_{RE}<5%), the mesh size should not be larger than 0.2 m. Thus, a mesh size of 0.2 m is adopted in the rest of the paper.

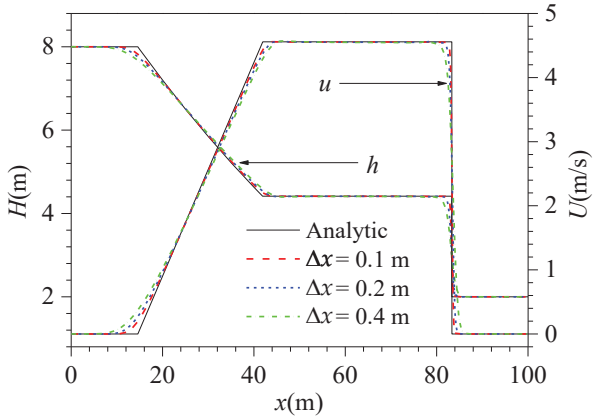

Fig. 4. Water depth and velocity profiles at t=4.0 s under different mesh sizes.

Table 2 : Errors at coupling interfaces under different mesh sizes (t=4.0 s).

Interface x_1	hx_1 (m)	AE (m)	RE (%)	ux_1(m/s)	AE (m)	RE (%)
Analytic	7.203	-	-	0.906	-	-
Δx =0.1 m	7.178	0.024	0.34	0.938	0.032	3.58
Δx =0.2 m	7.155	0.048	0.67	0.950	0.044	4.86
Δx =0.4 m	7.114	0.088	1.23	1.023	0.117	12.94
Interface x_2	hx_2 (m)	AE (m)	RE (%)	ux_2 (m/s)	AE (m)	RE (%)
Analytic	4.414	-	-	4.557	-	-
Δx =0.1 m	4.412	0.002	0.05	4.552	0.005	0.11
Δx =0.2 m	4.408	0.006	0.13	4.549	0.008	0.17
Δx =0.4 m	4.395	0.019	0.44	4.535	0.022	0.49

To access the spatial convergence order, the global relative errors L1 and L2 are defined as

$$L1 = \sqrt{\sum_{0}^{N} |u_i - u_a| \Big/ N}, \quad L2 = \sqrt{\sum_{0}^{N} (u_i - u_a)^2 \Big/ N} \tag{24}$$

where u_i is the simulated water velocity, u_a is the analytic solution, and N is the number of nodes.

Three mesh sizes, 0.1 m, 0.2 m, and 0.4 m, are selected, with each one doubled from the former. The convergence order of the 1D-2D coupled LB model is shown in **Fig. 5**. The convergence order of L1 and L2 are both around 1. The first-order convergence feature should be improved in later study because the standard order of LB models is second-order.

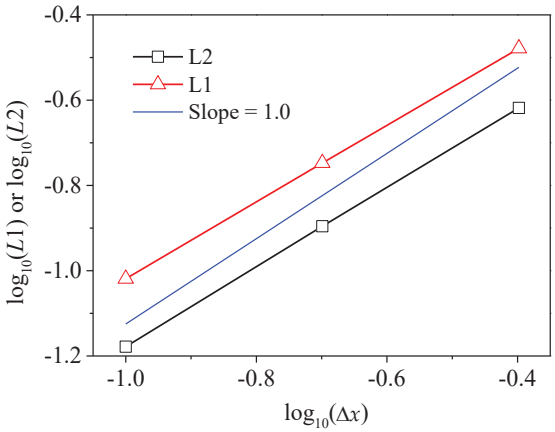

Fig. 5. Convergence order of the 1D-2D coupled LB model.

Numerical stability analysis

In this section, the numerical stability of the 1D-2D coupled LB model is analyzed. As indicated by a previous study [29], the relaxation time has a great influence on numerical stability. Therefore, we mainly analyze the effects of relaxation time parameters, tau1_up, tau1_down, and tau2. We set tau1_up to 0.5, 1.0, and 2.0, tau2 to 0.95, 1.1, 1.25, 1.4, and 1.55, and tau1_down to 0.7, 0.8, 0.85, 0.9, and 1.0. For all cases, the lattice length is 0.2 m and the time step is 0.01 s. Note that when the influence of one relaxation time is analyzed, the other two relaxation time parameters are fixed to the default values mentioned above.

As shown in **Fig. 6,** the results at interface x_1 are smooth and stable when tau1_up is ranging from 0.5 to 2.0, and the results are more accurate as the value of tau1_up closer to 0.5. This indicates that tau1_up has no obvious influence on numerical stability for negative waves.

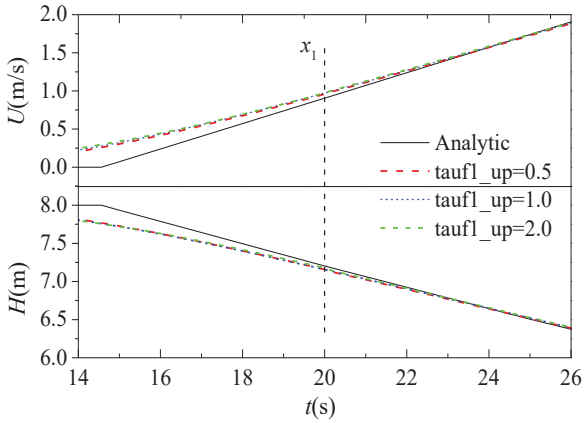

Fig. 6. The partial enlarged water depth and velocity profiles at t=4.0 s for different tau1_up.

Fig. 7 illustrates the influence of tau2 and tau1_down on numerical stability. The results show that both tau2 and tau1_down have an optimal relaxation time, which leading the smoothest connection at the coupling interface x_2. And the larger the relaxation time deviates from the optimal value, the larger the error at the connection. Therefore, the values of tau2 and tau1_down have a great influence on the numerical stability for advancing positive waves.

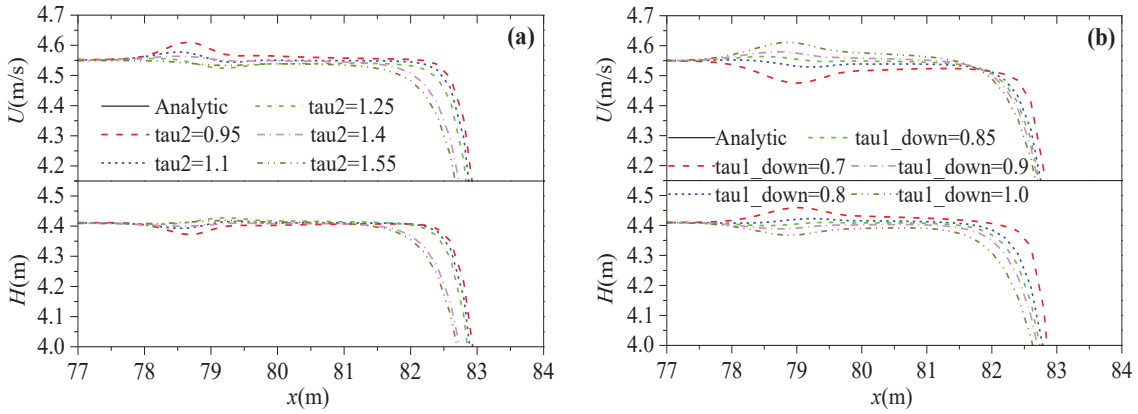

Fig. 7. Water depth and velocity profiles at t=4.0 s under different relaxation time tau2 and tau1_down: (a) the partial enlarged drawing for different tau2; (b) the partial enlarged drawing for different tau1_down.

The influence on the numerical stability of tau1_up is opposite with those of tau2 and tau1_down. The reasons can be illustrated as follows: the negative wave makes the water depth and velocity changed gradually at coupling interface x_1, while the progressive wave causes the water depth and velocity changed dramatically at coupling interface x_2. Therefore, the selection of the coupling interfaces should avoid the places where water depth and velocity change fast. If it cannot be avoided, the relaxation time should be reasonably selected to make the results as smooth as possible.

The surge waves in tailrace canal of a hydropower station

The surge waves in the tailrace canal of a hydropower station caused by load rejection is simulated by the 1D-2D coupled LB model. The tailrace canal has a constant rectangular cross-section with a length of 100 m, a width of 10 m, a flat bottom, and a roughness coefficient of 0.015. The upstream boundary is the given discharge, which decreases linearly from 600 m^3/s to 0.0 m^3/s within 8.0 s. The downstream boundary is a constant water depth of 15 m. As depicted in **Fig. 8**, the 2D model and 1D model is used to simulate the upstream half part and downstream half part of the domain, respectively, with the interface at x=50 m. The lattice length is 0.2 m, the time step is 0.01 s, and the relaxation time tau1=0.6 and tau2= 0.875.

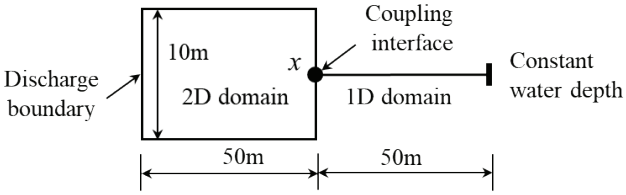

Fig. 8. Computational domain for the surge waves in the tailrace canal of a hydropower station.

The discharge and water depth histories at downstream, upstream, and interface x of the 1D-2D coupled LB model and Delft3D are compared in **Fig. 9**. The results agree well with each other, and the proposed method has a better ability to capture the steep inflection point of surge, indicating a smaller numerical diffusivity.

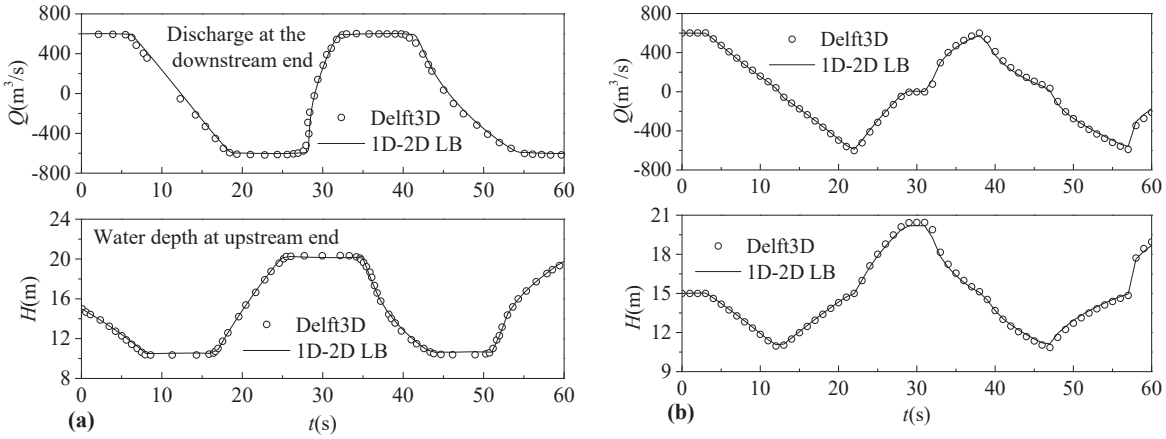

Fig. 9. Surge wave histories in the tailrace canal for load rejection: (a) water depth at the upstream end and discharge at the downstream end; (b) water depth and discharge histories at the coupling interface(x=50 m).

From the above analysis, the 1D-2D coupled LB model proven to be accurate and reliable. The choice of coupling interfaces should avoid the regions where shock waves or abrupt changes of flow field may occur. Otherwise, the LB relaxation time should be carefully tuned.

Simulation of surge waves in the reservoir of a run-of-river hydropower station

Computational setup

The surge wave propagation and reflection phenomena caused by a load rejection in a run-of-river hydropower station are simulated to further demonstrate the capability of the

present method. The hydropower station, the reservoir, and the computational domain are depicted in **Fig. 10**. The reservoir is divided into three parts (Channel 1 (C1), Channel 2 (C2) and channel 3 (C3)) by two dikes (Dike 1 (D1) and Dike 2 (D2)). There are two powerhouses (Powerhouse 1 (PH1) and Powerhouse 2 (PH2)) located at the end of Channel 2. Powerhouse 1 includes 14 turbines, with a total discharge of 11550 m^3/s, and Powerhouse 2 includes 7 turbines, with a total discharge of 6385 m^3/s. Channel 1 and Channel 3 are used for sand washing and shipping. There are two side branches: Branch 1 is 7.7 km, and Branch 2 is 2.2 km. Several monitoring points are set to record the flow parameters. Point A is located at the inlet of Powerhouse 1, Point B is located at the inlet of Powerhouse 2, Point C is located at the head of Dike 1, Point D is located at the head of Dike 2, Point E is located at estuary of Branch 1, Point F is located at estuary of Branch 2, and Point G is located at the coupling interface.

The simulation scope of this example is about 40 km, in which the 2D part of the reservoir (about 5 km starting from the dam to Point G) is treated by the 2D LB model, and the upstream 35 km river is handled by the 1D LB model. The upstream boundary of the 1D domain is set to constant discharge because there is a high dam located. The downstream boundary of the 2D domain is the dam, at which the discharge values of each powerhouse are given. Other boundaries are set to no-slip walls. The roughness of the river bed is 0.025. The time steps of 1D LB and 2D LB models are both set to 0.0864 s, and the corresponding uniform lattice length is 4.32 m. The mesh nodes are 8102 for the 1D domain and 1600×1200 for the 2D domain.

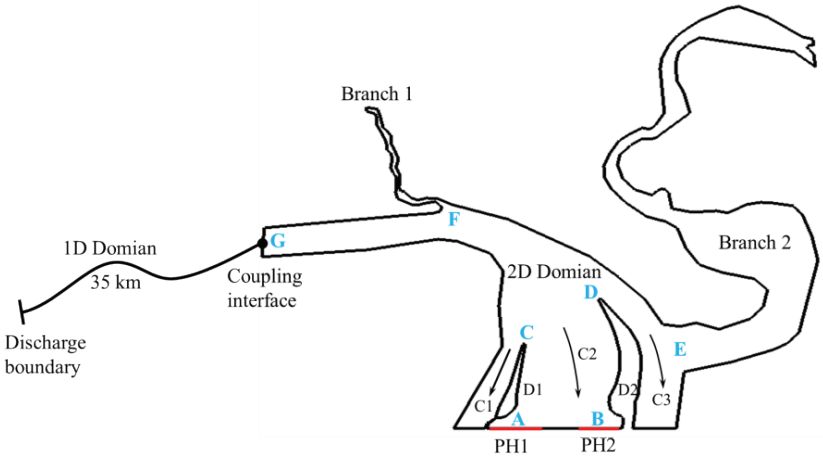

Fig. 10. Schematic of the reservoir region of the computational domain.

Simulation results

Steady flow simulation is conducted at the early stage of the simulation to use as the initial condition for the transient flow simulation. The transient process simulation is caused by the load rejection of all units in two powerhouses simultaneously, in which their discharge decrease linearly to zero within 40.0 s. The water depth and velocity at six typical moments are shown in **Fig. 11**.

After the load rejection, a pair of surge waves are generated from two powerhouses and propagated upstream (t=0.5 min). Then, the surge wave propagates back and forth between Dike 1 and Dike 2, causing the water depths near two dikes to fluctuate alternately. This

phenomenon is particularly obvious in the preliminary stages of this simulation (t=1.5 min and t=2.0 min). At about t=2.0 min, the surge wave reach the estuary of Branch 1 and Branch 2 for the first time. Meanwhile, it also reaches the front of Channel 1, which causes an obvious increase in water depth (t=3.0 min). The surge wave keeps propagating, at about t=3.5 min, it reaches the coupling interface. At about t=7.0 min, it arrives at the end of Branch 1.

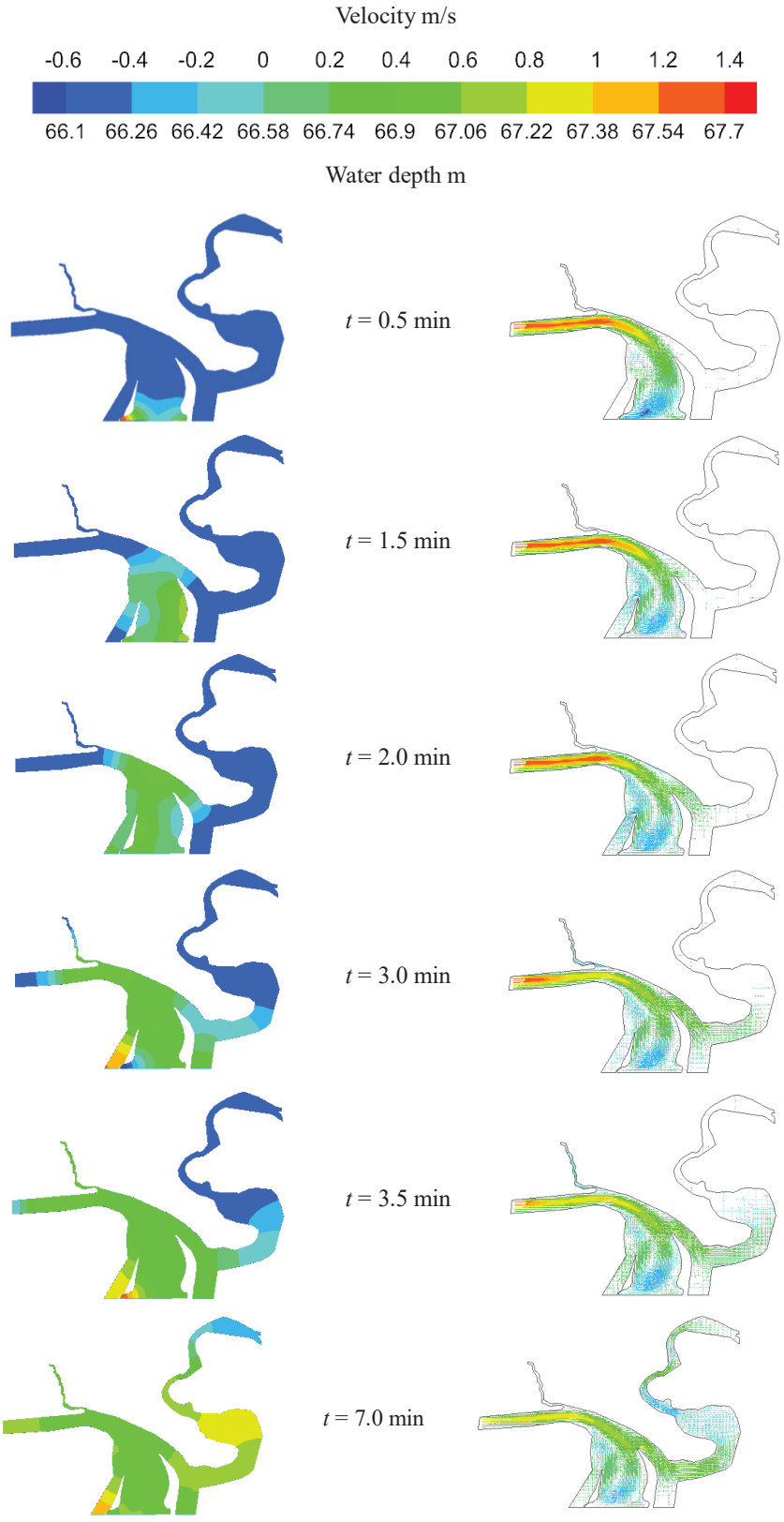

Fig. 11. Surge wave propagation and reflection in the reservoir after load rejection: water depth (left column) and velocity (right column).

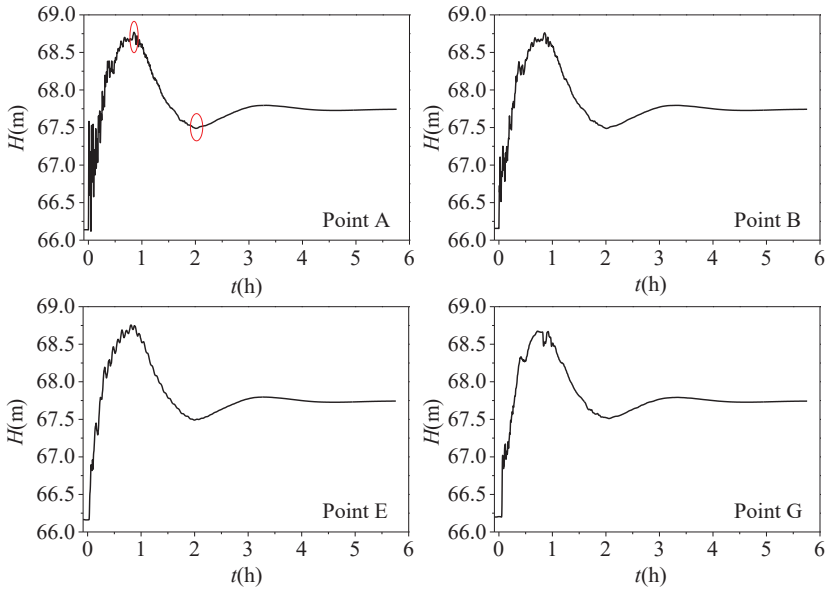

Fig. 12. Histories of the water depths for some monitoring points.

To analyze the water level fluctuations at each important building of the hydraulic project, **Fig. 12** shows the histories of water depth at the monitoring points. Many information can be extracted, such as the first moment affected by the surge waves, the maximum and the minimum water depths, and the attenuation duration of the surge waves. Take point A for example, the maximum and the minimum water depths are 68.77 m and 67.49 m, which occur around 0.85 and 2.0 hours, respectively. The time for the surge wave attenuating completely takes about 5.0 hours.

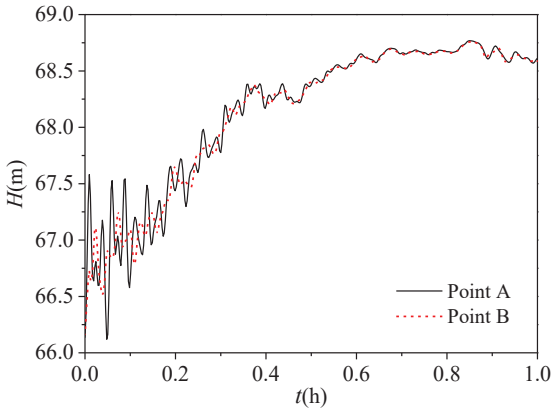

Fig. 13. Comparison of water depth at the inlets of Powerhouse 1 and Powerhouse 2.

To study the propagation and reflection rules of the surge waves, we enlarge the histories of water depth at the inlet of the two powerhouses. As shown in **Fig. 13**, the surge waves are composed of low frequency fundamental wave and high frequency wave. The former is due to the propagation and reflection of surge waves between the two powerhouses and upstream boundaries, and the latter is because of the wave propagation and reflection between dikes and banks. The riverbed resistance attenuates these waves gradually during the propagation processes. The high frequency wave disappears after 2.0 hours, and the low frequency fundamental wave dies out after 5.0 hours.

Computational efficiency analysis

The graphic processing unit (GPU) equipped with super-long pipeline and massive thread parallelism has shown powerful capability in non-graphical computations. The LB method has explicit and local features, which match the multi-thread parallel characteristics of GPU quite well. Thus, the 1D-2D coupled LB model can fully take advantage of the GPU to solve the computation-intensive problem.

To verify parallel computational efficiency, the 1D-2D coupled LB model is implemented on a GPU platform. The thread block is organized as a 1D array in both 1D and 2D computational domain, and the grid of 2D domain is organized as a 2D array that matches the plane expanded by two dimensions. Shared memory is used in the 2D computational domain because threads can concurrently access the shared memory at no cost as long as there are no bank conflicts.

Table 3 : Performance (in MNUPS) of the 1D-2D coupled LB model under different mesh sizes.

Lattice length (m)	2D Grid	1D Grid	Consumed time (h)	Performance	Speedup ratio
Δx =17.28	400×300	2026	0.71	17.09	-
Δx =8.64	800×600	4051	1.90	25.54	2.7
Δx =4.32	1600×1200	8102	4.47	43.12	6.3
Δx =2.16	3200×2400	16204	15.42	49.92	21.7

Four different mesh sizes 2.16 m, 4.32 m, 8.64 m, and 17.28 m, are simulated. The results are shown in **Table 3**, in which the time is given in hours and the performance is given in million nodes updated per second (MNUPS). All computations are carried out using double precision floating on an NVIDIA Geforce GTX TITAN X graphics card, which can deliver a peak performance of approximately 7×10^{12} single-precision floating point operations per second and a peak memory bandwidth of approximately 336.5 GB/s.

It can be seen that as the mesh becomes finer, the consumed time increases, but the performance and the speedup ratio increase, indicating that the coupled model can achieve better performances on finer meshes. Therefore, the 1D-2D coupled LB model has an outstanding advantage in the simulation of large-scale river-lake systems.

Conclusions

In this work, a novel 1D-2D coupled lattice Boltzmann model is developed for shallow water simulations in large scale river-lake systems. Both 1D and 2D models are numerically solved by the LB method. The coupling strategy is carried out at the mesoscopic level, in which the coupling interface is treated as an interior node of the 1D domain, and its unknown distribution functions are calculated by the macroscopic variables and the distribution functions at adjacent 1D and 2D nodes.

By verifying and applying the proposed model, we found that: (1) the 1D-2D coupled LB model has a good accuracy; (2) the numerical stability of the proposed model is greatly affected by the LB relaxation time, especially when water depth and velocity at the vicinity of the coupling interfaces change drastically. Thus, the placement of coupling interfaces should avoid the regions where shock waves or abrupt changes of flow field may occur. Otherwise, the LB relaxation time should be carefully tuned; (3) the coupled model can achieve better performances on finer meshes, indicating it has an enormous potential to simulate flows in large-scale river-lake systems.

The 1D-2D coupled LB model has a great value for applications because of its simple, high accuracy, convenient processing complex boundaries, suitable for parallel computing, and a wide application range. Further study for the 1D-2D coupled LB model will focus on its applications on simulations of water temperature and quality in large scale river-lake systems.

ACKNOWLEDGEMENTS

This work has been supported by the National Key Research and Development Program of China (Grant No. 2017YFC0405300).

REFERENCES

[1] Adeogun AG, Daramola MO, Pathirana A. Coupled 1D-2D hydrodynamic inundation model for sewer overflow: Influence of modeling parameters. Water Sci 2015;29:146–55. doi:10.1016/j.wsj.2015.12.001.

[2] Liu Q, Qin Y, Zhang Y, Li Z. A coupled 1D–2D hydrodynamic model for flood simulation in flood detention basin. Nat Hazards 2015;75:1303–25. doi:10.1007/s11069-014-1373-3.

[3] Morales-Hernández M, García-Navarro P, Burguete J, Brufau P. A conservative strategy to couple 1D and 2D models for shallow water flow simulation. Comput Fluids 2013;81:26–44. doi:10.1016/j.compfluid.2013.04.001.

[4] Meng W, Cheng Y, Wu J, Yang Z, Zhu Y. GPU Acceleration of Hydraulic Transient Simulations of Large-Scale Water Supply Systems. Appl Sci 2019;9:1–14. doi:10.3390/app9010091.

[5] Peng C, Geneva N, Guo Z, Wang LP. Direct numerical simulation of turbulent pipe flow using the lattice Boltzmann method. J Comput Phys 2018;357:16–42. doi:10.1016/j.jcp.2017.11.040.

[6] Silva G, Talon L, Ginzburg I. Low- and high-order accurate boundary conditions: From Stokes to Darcy porous flow modeled with standard and improved Brinkman lattice Boltzmann schemes. J Comput Phys 2017;335:50–83. doi:10.1016/j.jcp.2017.01.023.

[7] Fakhari A, Geier M, Lee T. A mass-conserving lattice Boltzmann method with dynamic grid refinement for immiscible two-phase flows. J Comput Phys 2016;315:434–57. doi:10.1016/j.jcp.2016.03.058.

[8] Cheng Y. Application of the lattice boltzmann method-one dimensional dam breaker simulation. Mech Eng (China) 2000;22:47–8.

[9] Cheng Y, Suo L. A lattice BGK lodel for simulating one-Dimensional unsteady open channel flows. Adv Water Sci (China) 2000;11:362–7. doi:10.14042/j .cnki .32.1309.2000.04.003.

[10] Frandsen JB. A simple LBE wave runup model. Prog Comput Fluid Dyn An Int J 2008;8:222-32. doi:10.1504/pcfd.2008.018093.

[11] van Thang P, Chopard B, Lefèvre L, Ondo DA, Mendes E. Study of the 1D lattice Boltzmann shallow water equation and its coupling to build a canal network. J Comput Phys 2010;229:7373–400. doi:10.1016/j.jcp.2010.06.022.

[12] Chopard B, Pham VT, Lefèvre L. Asymmetric lattice Boltzmann model for shallow water flows. Comput Fluids 2013;88:225–31. doi:10.1016/j.compfluid.2013.09.014.

[13] Zhou JG. A lattice Boltzmann model for the shallow water equations. Comput Methods Appl Mech Engrg 2002;191:3527–39.

[14] Cheng Y, Suo L. 2D open channel flow simulations by the lattice Boltzmann model. Adv Water Sci (China) 2003;14:9–14. doi:10.14042/j.cnki.32.1309.2003.01.002.

[15] Zhang C, Cheng Y, Wu J, Diao W. Lattice Boltzmann simulation of the open channel flow connecting two cascaded hydropower stations. J Hydrodyn 2016;28:400–10. doi:10.1016/S1001-6058(16)60643-1.

[16] Liu H, Zhou GJ, Burrows R. Lattice Boltzmann model for shallow water flows in curved and meandering channels. Int J Comut Fluid Dyn 2009;23:209–20. doi:10.1080/10618560902754924.

[17] Liu H, Zhu Z, Liu J, Liu Q. Numerical analysis of the impact factors on the flow fields in a large shallow lake. Water (Switzerland) 2019;11:1–13. doi:10.3390/w11010155.

[18] Liu H, Ding Y, Wang H, Zhang J. Lattice Boltzmann method for the age concentration equation in shallow water. J Comput Phys 2015;299:613–29. doi:10.1016/j.jcp.2015.07.022.

[19] Ding Y, Liu H, Peng Y, Xing L. Lattice Boltzmann method for rain-induced overland flow. J Hydrol 2018;562:789–95. doi:10.1016/j.jhydrol.2018.05.017.

[20] Chen Y, Wang Z, Liu Z, Zhu D. 1D–2D Coupled Numerical Model for Shallow-Water Flows. J Hydraul Eng 2011;138:122–32.

[21] Kuiry S, Sen D, Bates PD, Yan D. Application of the 1d-quasi 2d model tinflood for floodplain inundation prediction of the river thames. ISH J Hydraul Eng 2011;17:98–110. doi:10.1080/09715010.2011.10515036.

[22] Marin J, Monnier J. Superposition of local zoom models and simultaneous calibration for 1D – 2D shallow water flows 2009;80:547–60. doi:10.1016/j.matcom.2009.09.001.

[23] Fernández-Nieto ED, Marin J, Monnier J. Coupling superposed 1D and 2D shallow-water models: Source terms in finite volume schemes. Comput Fluids 2010;39:1070–82. doi:10.1016/j.compfluid.2010.01.016.

[24] Steinebach G, Rademacher S, Rentrop P, Schulz M. Mechanisms of coupling in river flow simulation systems. J Comput Appl Math 2004;168:459–70. doi:10.1016/j.cam.2003.12.008.

[25] Miglio E, Perotto S, Saleri F. Model coupling techniques for free-surface flow problems: Part i. Nonlinear Anal Theory, Methods Appl 2005;63:1885–96. doi:10.1016/j.na.2005.03.083.

[26] Twigt DJ, De Goede ED, Zijl F, Schwanenberg D, Chiu AYW. Coupled 1D-3D hydrodynamic modelling, with application to the Pearl River Delta. Ocean Dyn 2009;59:1077–93. doi:10.1007/s10236-009-0229-y.

[27] Zhang XX, Cheng YG, Yang JD, Xia LS, Lai X. Simulation of the load rejection transient process of a francis turbine by using a 1-D-3-D coupling approach. J Hydrodyn 2014;26:715–24. doi:10.1016/S1001-6058(14)60080-9.

[28] Bladé E, Gómez-Valentín M, Dolz J, Aragón-Hernández JL, Corestein G, Sánchez-Juny M. Integration of 1D and 2D finite volume schemes for computations of water flow in natural channels. Adv Water Resour 2012;42:17–29. doi:10.1016/j.advwatres.2012.03.021.

[29] Thorimbert Y, Lätt J, Chopard B. Coupling of lattice Boltzmann shallow water model with lattice Boltzmann free-surface model. J Comput Sci 2019;33:1–10. doi:10.1016/j.jocs.2019.01.006.

[30] Guo Z, Zheng C. Theory and Applications of Lattice Boltzmann Method. Beijing: Science Press; 2009.

[31] He Y, Wang Y, Li Q. lattice Boltzmann Method: Theory and Application. Beijing: Science Press; 2009.

[32] Ginzburg I. Multiple-relaxation-time lattice Boltzmann. R Soc 2002;360:437–51.

[33] Cheng Y, Li J. Introducing unsteady non-uniform source terms into the lattice Boltzmann model. Int J Numer Methods Fluids 2008;56:629–41. doi:10.1002/fld.

[34] Chen H, Chen S, Matthaeus WH. Recovery of the Navier-Stokes equations using a lattice-gas Boltzmann method. Phys Rev A 1992;45:5339–42. doi:10.1103/PhysRevA.45.R5339.

[35] Zou Q, He X. On pressure and velocity flow boundary conditions and bounceback for the lattice Boltzmann BGK model. Phys Fluids 1997;9:1591–8. doi:10.1063/1.869307.

[36] Stoker JJ. The Formation of Breakers and Bores. Commun Pure Appl Math 1948;1:1–87.